Video Article

A Rapid Synthesis Method for Au, Pd, and Pt Aerogels Via Direct Solution-Based Reduction

Fred J. Burpo[1], Enoch A. Nagelli[1], Lauren A. Morris[2], Joshua P. McClure[3], Madeline Y. Ryu[1], Jesse L. Palmer[1]

[1]Department of Chemistry and Life Science, United States Military Academy, West Point

[2]Armament Research, Development and Engineering Center, U.S. Army RDECOM-ARDEC

[3]Sensors and Electron Devices Directorate, United States Army Research Laboratory

Correspondence to: Fred J. Burpo at john.burpo@usma.edu

URL: https://www.jove.com/video/57875
DOI: doi:10.3791/57875

Keywords: Chemistry, Issue 136, aerogel, porous, gold, palladium, platinum, catalysis

Date Published: 6/18/2018

Citation: Burpo, F.J., Nagelli, E.A., Morris, L.A., McClure, J.P., Ryu, M.Y., Palmer, J.L. A Rapid Synthesis Method for Au, Pd, and Pt Aerogels Via Direct Solution-Based Reduction. *J. Vis. Exp.* (136), e57875, doi:10.3791/57875 (2018).

Abstract

Here, a method to synthesize gold, palladium, and platinum aerogels via a rapid, direct solution-based reduction is presented. The combination of various precursor noble metal ions with reducing agents in a 1:1 (v/v) ratio results in the formation of metal gels within seconds to minutes compared to much longer synthesis times for other techniques such as sol-gel. Conducting the reduction step in a microcentrifuge tube or small volume conical tube facilitates a proposed nucleation, growth, densification, fusion, equilibration model for gel formation, with final gel geometry smaller than the initial reaction volume. This method takes advantage of the vigorous hydrogen gas evolution as a by-product of the reduction step, and as a consequence of reagent concentrations. The solvent accessible specific surface area is determined with both electrochemical impedance spectroscopy and cyclic voltammetry. After rinsing and freeze drying, the resulting aerogel structure is examined with scanning electron microscopy, X-ray diffractometry, and nitrogen gas adsorption. The synthesis method and characterization techniques result in a close correspondence of aerogel ligament sizes. This synthesis method for noble metal aerogels demonstrates that high specific surface area monoliths may be achieved with a rapid and direct reduction approach.

Video Link

The video component of this article can be found at https://www.jove.com/video/57875/

Introduction

A wide range of energy storage and conversion, catalysis, and sensor applications benefit from three-dimensional metallic nanostructures which provide control over chemical reactivity, and mass transport properties[1,2,3,4,5]. Such 3-dimensional metallic nanostructures further enhance conductivity, ductility, malleability, and strength[8,9]. Integration into devices necessitates that materials be free-standing or combined with support materials. Incorporation of nanomaterials onto support structures provides a means of minimizing active material, but may suffer from weak adsorption and eventual agglomeration during device operation[10,11].

While there are a variety of synthesis methods to control individual nanoparticle size and shape, few approaches enable control over contiguous 3-dimensional nanomaterials[12,13,14]. Noble metal 3-dimensional nanostructures have been formed through dithiol linkage of monodisperse nanoparticles, sol-gel formation, nanoparticle coalescence, composite materials, nanosphere chains, and biotemplating[15,16,17,18]. Many of these approaches require synthesis times on the order of days to weeks to yield desired materials. Noble metal nanofoams synthesized from the direct reduction of precursor salt solutions have been prepared with a faster synthesis timescale and with short-range order of hundreds of micrometers in length, but require mechanical pressing for device integration[19,20].

First reported by Kistler, aerogels provide a synthesis route to achieve porous structures with high specific surface areas that are orders of magnitude less dense than their bulk material counterparts[21,22,23]. Extending 3-dimensional structures to the macroscopic length scale of bulk materials offers an advantage over nanoparticle aggregates or nanofoams that require support materials or mechanical processing. While aerogels provide a synthesis route to control porosity and particle feature size, however, extended synthesis times, and in some cases the use of capping agents or linker molecules, increases overall processing steps and time.

Here a method to synthesize gold, palladium, and platinum aerogels via a rapid, direct solution-based reduction is presented[24]. Combining various precursor noble metal ions with reducing agents in a 1:1 (v/v) ratio results in the formation of metal gels within seconds to minutes compared to much longer synthesis times for other techniques such as sol-gel. The use of a microcentrifuge tube or small volume conical tube takes advantage of the vigorous hydrogen gas evolution as a by-product of the reduction step facilitating a proposed nucleation, growth, densification, fusion, equilibration model for gel formation. A close correlation in aerogel nanostructure feature sizes is determined with scanning electron microscopy image analysis, X-ray diffractometry, nitrogen gas adsorption, electrochemical impedance spectroscopy, and cyclic voltammetry. The solvent accessible specific surface area is determined with both electrochemical impedance spectroscopy and cyclic

voltammetry. This synthesis method for noble metal aerogels demonstrates that high specific surface area monoliths may be achieved with a rapid and direct reduction approach.

Protocol

CAUTION: Consult all relevant safety data sheets (SDS) before use. Use appropriate safety practices when performing chemical reactions, to include the use of a fume hood and personal protective equipment. Rapid hydrogen gas evolution can cause high pressure in reaction tubes causing caps to pop and solutions to spray out. Ensure that reaction tube caps remain open as specified in the protocol.

1. Metal Gel Preparation

1. **Preparation of metal ion solutions.**
    1. Prepare 2 mL of 0.1 M solutions of the following salts: $HAuCl_4 \cdot 3H_2O$ and Na_2PdCl_4 in deionized water. Prepare 2 mL of 0.1 M K_2PtCl_6 in a 1:1 (v/v) water and ethanol solvent. Vigorously shake and vortex solutions to aid in the dissolution of the salts.

2. **Preparation of reducing agent solutions.**
    1. Prepare 10 mL of 0.1 M solutions of the following reducing agents: dimethylamine borane (DMAB) and $NaBH_4$ (sodium borohydride).

3. **Preparation of Au gels.**
    1. Pipette 0.5 mL of 0.1 M $HAuCl_4 \cdot 3H_2O$ solution into a 1.7 mL or 2.0 mL microcentrifuge tube. Forcefully pipette 0.5 mL of DMAB into the microcentrifuge tube with gold solution to ensure a rapid mix of salt and reducing agent solutions. Once the solutions are mixed, place the microcentrifuge tube vertically in a tube rack with the tube cap open.
    Note: If the tube cap is left closed, hydrogen gas evolution will cause the pressure inside to force the cap to pop open and potentially spray the reduction mixture.

4. **Preparation of Pd gels.**
    1. Pipette 0.5 mL of 0.1 M Na_2PdCl_4 solution into a 1.7 mL or 2.0 mL microcentrifuge tube. Forcefully pipette 0.5 mL of $NaBH_4$ into the microcentrifuge tube with palladium solution. Place the microcentrifuge tube vertically in a tube rack with the tube cap open.

5. **Preparation of Pt gels.**
    1. Pipette 0.5 mL of 0.1 M K_2PtCl_6 solution into a 1.7 mL or 2.0 mL microcentrifuge tube. Forcefully pipette 0.5 mL of DMAB into the microcentrifuge tube with platinum solution. Place the microcentrifuge tube vertically in a tube rack with the tube cap open.

6. **Tube inversion.**
    1. At approximately 5 min, cap the microcentrifuge tubes and gently invert 3-5 times to aid in the coalescence of metal particles not part of the metal gel. Ensure that the tube caps are immediately uncapped after inverting tubes, and replace tubes in a rack to maintain the vertical orientation of the tube.

7. **Equilibration**.
    1. While Au, Pd, and Pt gels initially form within minutes, leave nascent gels in reducing agent solution for 3 – 6 h to allow for complete reduction of metal ions and for surface free energy minimization to occur.
    Note: Metal gels occupy a smaller volume than the initial volume of mixed metal ion and reducing agent solution. Some additional slight volume contraction may be observed during equilibration time, and is more pronounced for gold gels and believed to be due to Ostwald ripening[25].

8. **Gel rinsing**.
    1. For Au, Pd, and Pt gels after the equilibration period, remove excess reducing agent solution, but leave enough solution volume so that the metal gel remains submerged. Ensure that the solution meniscus does not come in contact with the metal gel.
    Note: Although the metal gels are stable enough to transfer between solutions with a spatula, capillary forces due to contact with the solution meniscus will deform and compress the gels resulting in an increase in the final aerogel density. This requires that some reducing agent solution remains in the tube with the gel submerged when transferring to deionized water.
    2. Slowly pipette deionized water to the top of the reaction microcentrifuge tubes. Submerge the microcentrifuge tube in a 50 mL conical tube full of deionized water and allow the gel to slide out of the microcentrifuge tube.
    3. Leave the gel in the deionized water for 24 h, and replace the water at 12 h. Do not to allow a liquid meniscus to come in contact with the gel.

2. Electrochemical Surface Area (ECSA) Characterization of Wet Metal Gels

Note: Electrochemical characterization is performed on wet metal gels prior to conducting freeze drying. The resulting ECSA is then an estimate of the surface of the final aerogel structure. Nitrogen adsorption measurements are used to estimate the surface area of the dried aerogels.

1. **Solvent exchange**.
    1. Remove as much of the deionized water from the Au, Pd, and Pt rinse solutions as possible and ensure that the liquid meniscus does not come in contact with the gel.
    2. Add 50 mL, 0.5 M KCl to the conical tubes in order to exchange the deionized water with supporting electrolyte within the gel pores. Leave the gels in KCl solution for 24 h.

2. **Working electrode preparation.**

1. Coat a 1 mm platinum wire electrode with non-reactive lacquer using a fine bristle brush or other application device leaving a 4-5 mm length of the wire tip exposed.
2. Allow 20 minutes for the lacquer to dry.
3. Apply at least two coats of lacquer.

3. **3-electrode cell set-up.**
   1. Use a 3-electrode cell set-up with an Ag/AgCl (3 M saturated) reference electrode, a 0.5 mm diameter Pt wire auxiliary/counter electrode, and the lacquer coated working electrode.
   2. Cut a plastic 50 mL conical tube in half and use as an electrochemical vial.
   3. Contact the gel with the working electrode with one of two methods: 1) impaled gel, or 2) contact mode.
      1. **Working electrode - impaled gel**.
         1. With the gel at the bottom of the modified 50 mL conical tube, gently insert the lacquer coated electrode into the gel.
            Note: The impaled gel method proves more effective with Au gels, whereas Pd and Pt gels fracture more frequently upon electrode insertion.

      2. **Working electrode - contact mode**.
         1. Insert the lacquer coated working electrode into the conical tube along the inner surface and rest the metal gel on the top of the exposed Pt wire of the working electrode.

4. **Electrochemical impedance spectroscopy (EIS)**.
   1. Perform potentiostatic EIS scans with frequencies between 100 MHz and 1 mHz using a 10 mV amplitude sine wave. In the event of current overflows, use galvanostatic EIS with the same frequency range and a 100 – 200 mA amplitude sine wave.

5. **Determination of electrochemical surface area (ECSA) from EIS data**.
   1. For Z'', the imaginary component of impedance, at the lowest EIS frequency f of 1 mHz, and dividing by the sample mass, m, use the following equation to determine specific capacitance, C_{sp}:
      $C_{sp} = 1/(2\pi f Z'' m)$ (1)
      Note: Given that the ECSA is determined from a wet gel prior to freeze drying in Step 3 below, determine mass by assuming all of the metal ions in solution are reduced to form the gel. Based on this assumption, any actual yield less than 100% will result in underestimating C_{sp}.

6. **Cyclic voltammetry (CV)**.
   1. Use scan rates of 100, 75, 50, 25, 10, 5, and 1 mV/s for CV measurements. Use voltage ranges of -0.2 to 0.2 V (vs Ag/AgCl) for Au gels, and select 0.1 to 0.4 V for Pd and Pt gels to avoid hydrogen adsorption and desorption, and oxidation-reduction of the metals.

7. **Determination of electrochemical surface area (ECSA) from CV data**.
   1. Use the slowest CV scan rate of 1 mV/s, and calculate specific capacitance with the equation:
      $C_{sp} = (\int iv dv) / (2\mu m \Delta V)$ (2)
      Note: Here i and v are the current and potential in the CV scan (A and V), scan rate is μ (V/s), mass of the gel is m (g), and ΔV is the potential window of discharge (vs Ag/AgCl).

3. Aerogel Preparation and Characterization.

1. Remove the deionized rinse water for Au, Pd, and Pt gels in Step 1.8 and ensure that the water meniscus does not come in contact with the metal gels.
2. Place the gels in a -80 °C freezer for no less than 30 min. Transfer the frozen metal gels to a freeze dryer with a set point pressure of 4 Pa or lower.

Representative Results

The addition of metal ion and reducing agent solutions together results in solutions immediately turning a dark black color with vigorous gas evolution. Observation of the reaction progress suggests the proposed gel formation mechanism shown in **Figure 1**. Gel formation proceeds through five steps of 1) nanoparticle nucleation, 2) growth, 3) densification, 4) fusion, and 5) equilibration. The first four steps are observed to occur during the first few minutes of the reaction, with the equilibration fifth step proceeding during the 3-6 h while the gel remains in the reducing agent solution, and continues during the deionized water rinse. **Figure 2** shows representative Au, Pd, and Pt aerogels floating on the surface of water indicating a characteristic aerogel hydrophobicity. Pd and Pt gels remained black in color from the initial combination of metal ion and reducing agent solutions, whereas gold gels progressed from black at initial reduction to presenting a red-gold hue during the equilibration phase.

Figure 3 photo images depict wet metal gels after reduction with reducing agent solution replaced with deionized water. A range of metal ion solution concentrations less than the 0.1 M presented in Step 1 of the Protocol section were reduced with the same 0.1 M reducing agent concentrations. For the combinations of $HAuCl_4 \cdot 3H_2O$ with DMAB, Na_2PdCl_4 with $NaBH_4$, and K_2PtCl_6 (in 50% ethanol) with DMAB, and metal ion concentrations of 5, 10, 25, 50, and 100 mM, gel size was found to decrease with decreasing metal ion concentration. The synthesis method presented here provides the significant advantage of rapid time scales to achieve the aerogel monoliths. However, the final gel size for 0.1 M metal concentrations is seen to be approximately ¼ to ⅓ of the synthesis solution volume. The gel formation mechanism facilitated by rapid hydrogen gas evolution results in fast gel formation, but ultimately results in a lack of shape control for this method.

To test the range of possible gel formation outcomes, various combinations of noble metal ions with three reducing agents were tested using the method presented in Protocol Step 1. The three reducing agents used were DMAB, $NaBH_4$, and sodium hypophosphite (NaH_2PO_2). All reducing agents were used at 0.1 M concentration. The metal salts used were $HAuCl_43H_2O$, Na_2PdCl_4, $Pd(NH_3)_4Cl_2$, K_2PtCl_4, $Pt(NH_3)_4Cl_2$, and Na_2PtCl_6. Na_2PtCl_6 was prepared with deionized water and separately with a 1:1 deionized water to ethanol solvent. Metal ion concentrations were varied across a range of 100, 50, 25, 10, 5, 1, 0.5, and 0.1 mM. **Table 1** indicates the minimum metal ion concentration at which gel formation was observed to occur. The metal ions and reducing agent combinations presented in Protocol step 1 resulted in the most reproducible and stable gels. While Au gels formed with the use of $NaBH_4$, gel shapes were more varied and presented a rougher macroscopic surface texture. Pd gels formed with Na_2PdCl_4 and $Pd(NH_3)_4Cl_2$ yielded similar results. Stable Pt gels were difficult to achieve using $Pt(NH_3)_4Cl_2$ and K_2PtCl_4 likely owing to the thermodynamic stability of the square planar platinum ions. Large gel aggregates formed with Na_2PtCl_6 prepared in deionized water solvent, whereas the use of Na_2PtCl_6 prepared in a 1:1 deionized water to ethanol solvent more consistently resulted in monolithic gels. The addition of ethanol as a solvent was based on reports of Pt nanoparticle instability in ethanol to drive particle aggregation and fusion. In general, gel shape became more variable for decreasing precursor salt concentrations for Au, Pd, and Pt.

Scanning electron microscope (SEM) analysis of the gels reveals a hierarchical pore structure for Au, Pd, and Pt aerogels as seen in **Figure 4**. The range of pore and ligament sizes were determined from SEM image analysis with 200 - 300 measurements for each value. Au aerogels present large macropores with a range of 50 - 600 nm, and smooth ligaments with a diameter range of 18 - 280 nm with an average of 63.7 ± 36.0 nm. Pd and Pt aerogels differ in their structure from Au aerogels, in that they present a "beads-on-a-string" structure with fused nanoparticles. Pd macropores ranged from 50 - 340 nm, with ligament diameters ranging from 12 - 65 nm, with an average of 34.5 ± 9.5 nm. Pt macropores range from 50 - 470 nm, with ligament diameters ranging from 13 - 60 nm, with an average of 29.7 ± 9.0 nm[24]. The greater range in Pt macropore structure is attributed to Pt nanoparticle stability and the need for ethanol to drive coalescence, and consequent ease of large hydrogen gas bubble evolution during the gel formation process. X-ray diffraction (XRD) spectra from 20 - 70 ° in **Figure 5** indicate characteristic peaks for Au, Pd, and Pt aerogels with no detectable oxides.

Nitrogen gas physisorption isotherms are shown for Au, Pd, and Pt aerogels in **Figure 6a**, **6c**, and **6e**, and indicate a Type IV isotherm characteristic of mesoporous materials with pores predominantly ranging from 2 – 50 nm[28] . The Barrett–Joyner–Halenda (BJH) model for desorption curves was used for **Figure 6b**, **6d**, and **6f** to show the cumulative pore volume (cm^3/g) and pore size distribution (dV/dd) for Au, Pd, and Pt aerogels with pore sizes in the 2 – 50 nm mesoporous range[29] . To determine the aerogel specific surface areas, a multi-point Brunauer-Emmett-Teller (BET) model was used to analyze adsorption isotherms in **Figure 6**.[30] For Au, Pd, and Pt aerogels this resulted in values of 3.06, 15.43, and 20.56 m^2/g respectively. Noble metal aerogels synthesized from sol-gels of preformed nanoparticles have achieved similar specific surface areas[31]. Idealized ligament diameters based on the specific surface areas are 85.4, 33.1, and 13.6 nm for Au, Pd and Pt aerogels and generally correlate to feature sizes determined with SEM image analysis.

Electrochemical impedance spectra for Au, Pd, and Pt gels are shown in **Figure 7a**. Specific capacitance is plotted as a function of EIS frequency in **Figure 7b** with estimates of 2.18. 4.13, and 4.20 F/g for Au, Pd, and Pt gels. Based on a nominal 30 $\mu F/cm^2$ for metal surfaces, Au, Pd, and Pt specific surface areas are 7.27, 13.77, and 14.00 m^2/g[32]. EIS spectra were fit with a transmission line model (TLM) based on a modified Randle's equivalent circuit model shown in **Figure 7c**. In this model, resistors (R), capacitors (C) or constant phase elements (CPE), and restricted diffusion elements (Z_{diff}) are connected in parallel and series. Electrolyte resistance and contact resistance with the working electrode at high frequency is represented by R1. Double layer capacitance, charge transfer, material resistance, and restricted ion diffusion through the hierarchically distributed pore network is represented by the parallel arrangement of CPE or C elements with serially connected R and Z_{diff}[33,34]. The TLM model effectively modeled EIS spectra for Au, Pd, and Pt gels.

Cyclic voltammetry scans are shown in **Figure 8a-8c** for Au, Pd, and Pt gels respectively. Using the 1 mV/s CV scan rate, specific capacitances for Au, Pd, and Pt gels were calculated to be 2.67, 7.99, and 5.12 F/g, and using the nominal value of 30 $\mu F/cm^2$, the same as for EIS capacitances, yields specific surface areas 8.90, 26.63, and 17.07 m^2/g.

	Reducing Agent		
Salt	**DMAB**	**$NaBH_4$**	**$NaHPO_2$**
	100 mM	**100 mM**	**100 mM**
$[AuCl_4]^-$	10 mM	5 mM	No Gel
$[Pd(NH_3)_4]^{2+}$	25 mM	5 mM	No Gel
$[PdCl_4]^{2-}$	25 mM	5 mM	50 mM
$[Pt(NH_3)_4]^{2+}$	No Gel	100 mM	No Gel
$[PtCl_4]^{2-}$	No Gel	100 mM	No Gel
$[PtCl_6]^{2-}$	25 mM	No Gel	No Gel
$[PtCl_6]^{2-}$	10 mM	No Gel	No Gel
50% EtOH			

Table 1. Concentration thresholds for gel formation for different combinations of salt type and reducing agents. Reproduced from reference 24 with permission.

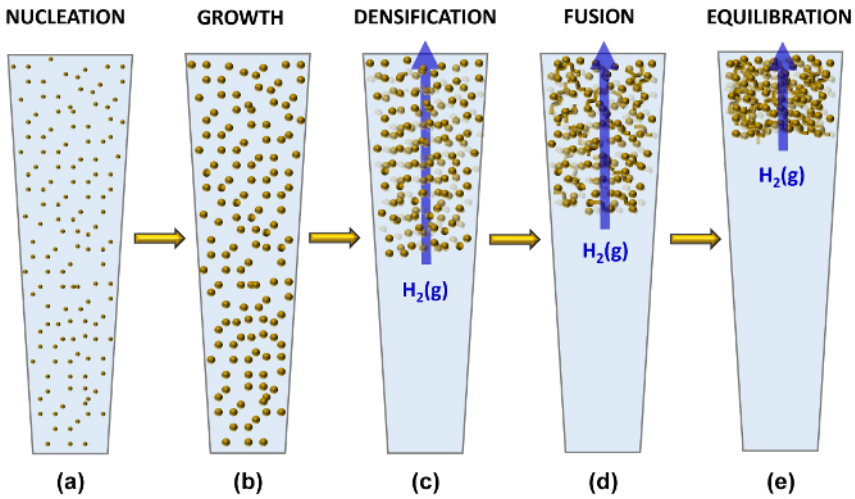

Figure 1. Proposed mechanism of noble metal gel formation. Synthesis proceeds via (a) initial nucleation of nanoparticles, (b) rapid growth of nanoparticles, (c) densification of nanoparticles due to hydrogen gas evolution, (d) fusion of nanoparticles, and finally (e) surface free energy minimization and equilibration of resulting gel. Reproduced from reference 24 with permission. Please click here to view a larger version of this figure.

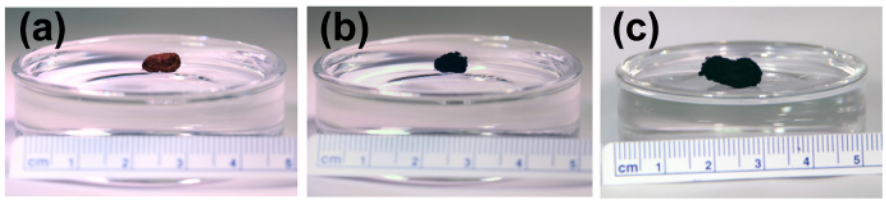

Figure 2. (a) Gold, (b) palladium, and (c) platinum aerogels floating on water. Modified from reference 24 with permission. Please click here to view a larger version of this figure.

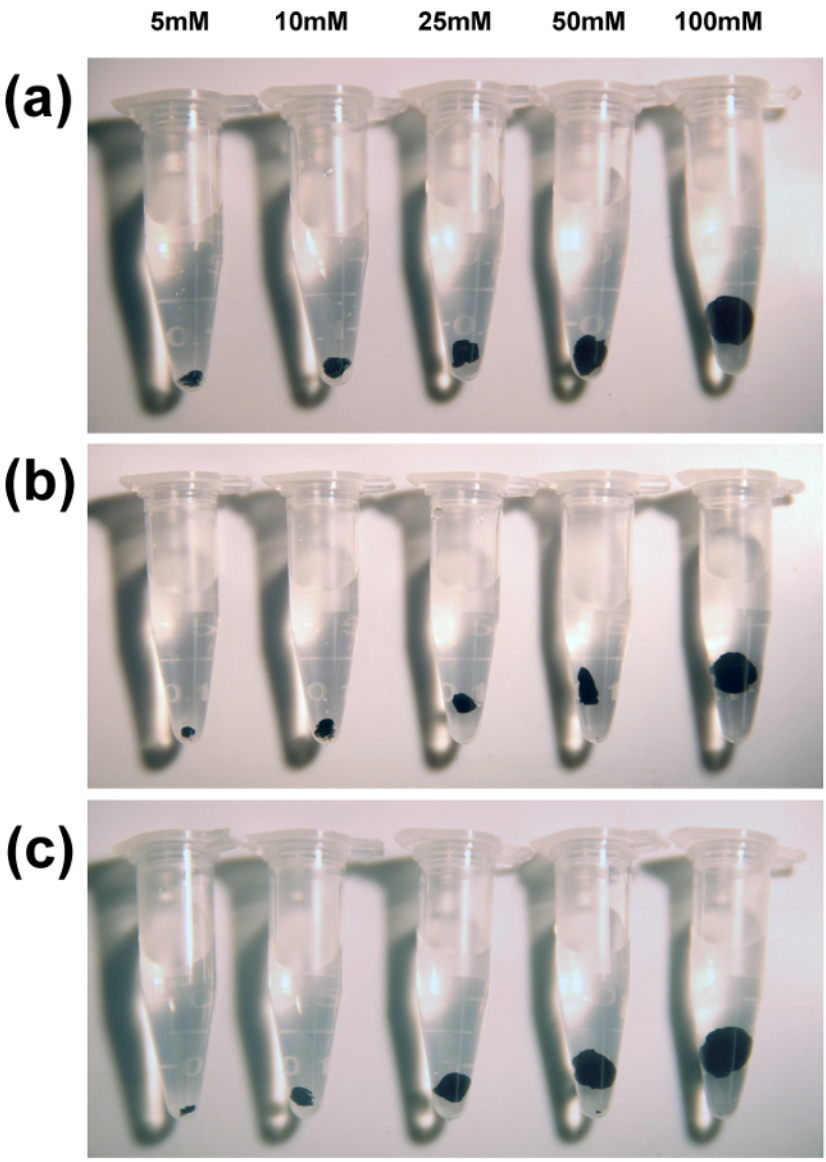

Figure 3. Noble metal gel synthesis across a range of salt concentrations from right to left of 100, 50, 25, 10, and 5 mM. (a) $[AuCl_4]^-$ reduced with 100 mM DMAB. (b) $[PdCl_4]^{2-}$ reduced with 100 mM $NaBH_4$. (c) $[PtCl_6]^{2-}$ prepared in 50% ethanol, reduced with 100 mM DMAB. Modified from reference 24 with permission. Please click here to view a larger version of this figure.

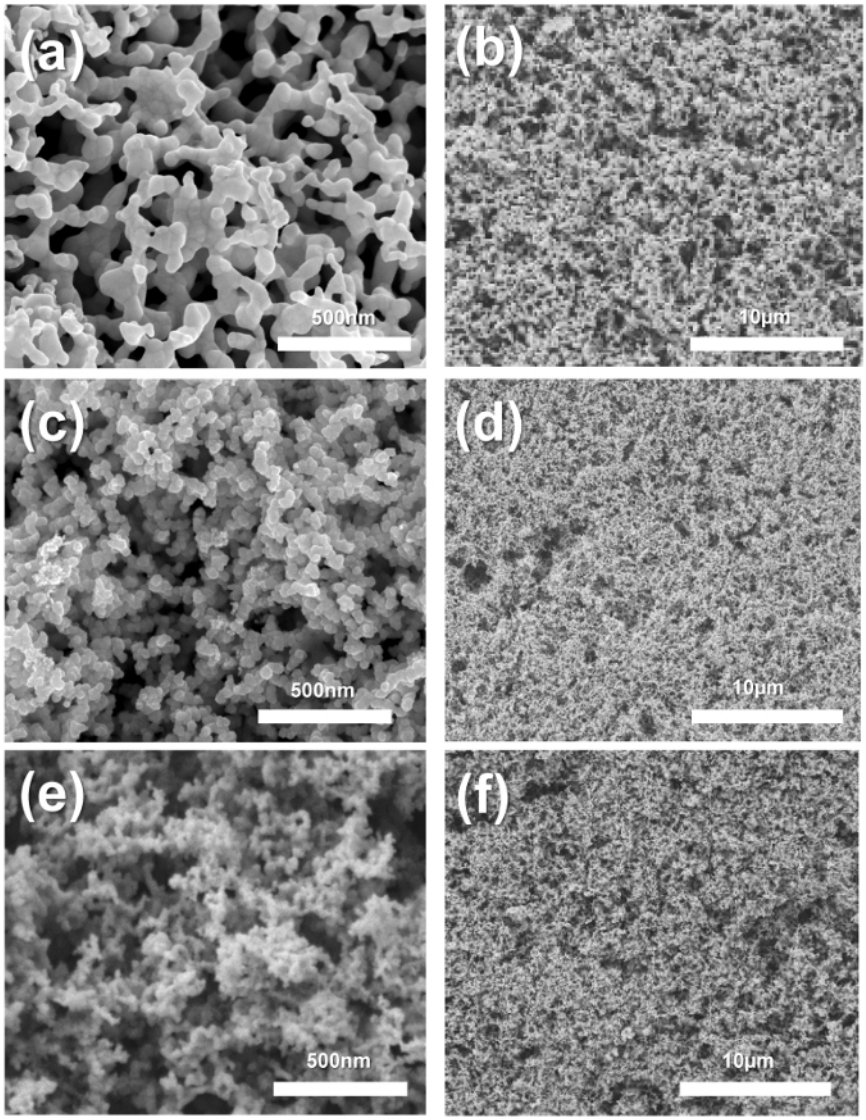

Figure 4. Scanning electron micrographs of (a)-(b) gold, (c)-(d) palladium, and (e)-(f) platinum aerogels. Reproduced from reference 24 with permission. Please click here to view a larger version of this figure.

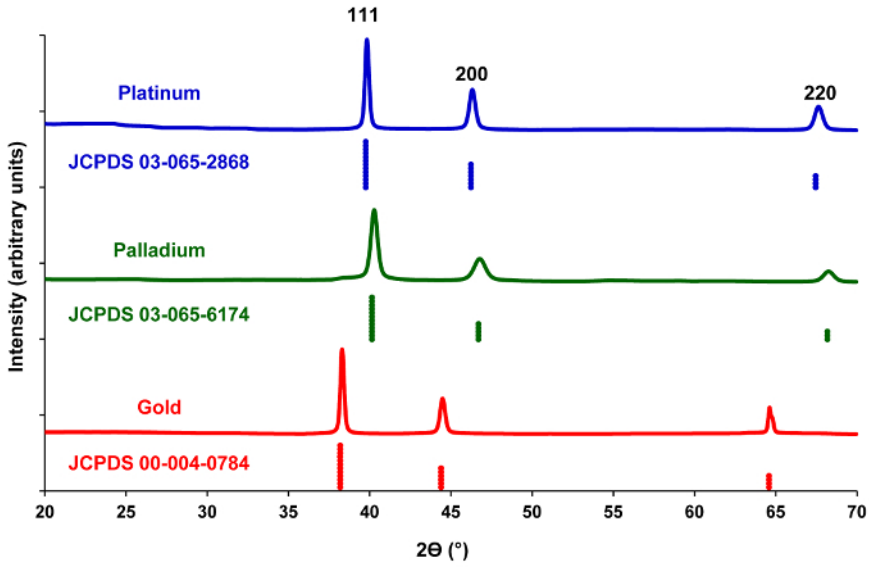

Figure 5. XRD spectra for platinum (top), palladium (middle), and gold (bottom) aerogels. Modified from reference 24 with permission. Please click here to view a larger version of this figure.

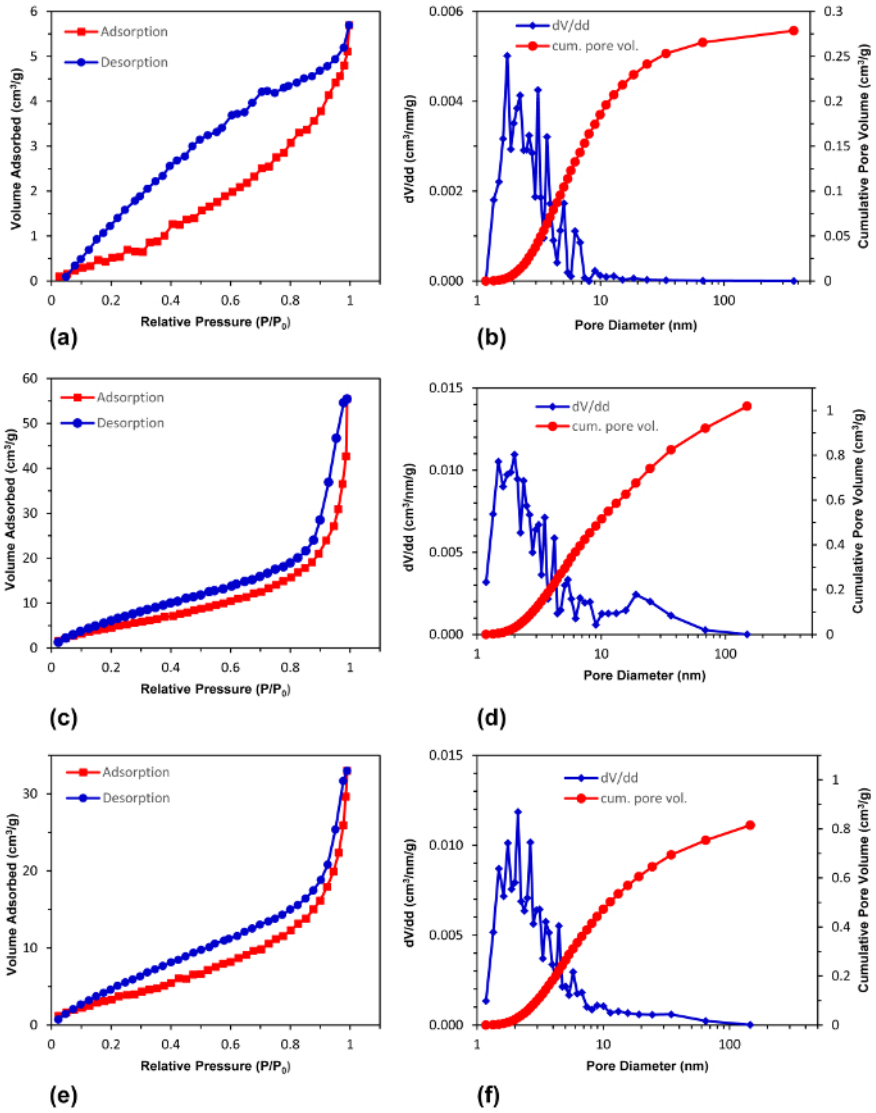

Figure 6. Nitrogen adsorption-desorption isotherms, and pore size distribution with cumulative pore volume for (a)-(b) gold, (c)-(d) palladium, and (e)-(f) platinum aerogels. Reproduced from reference 24 with permission. Please click here to view a larger version of this figure.

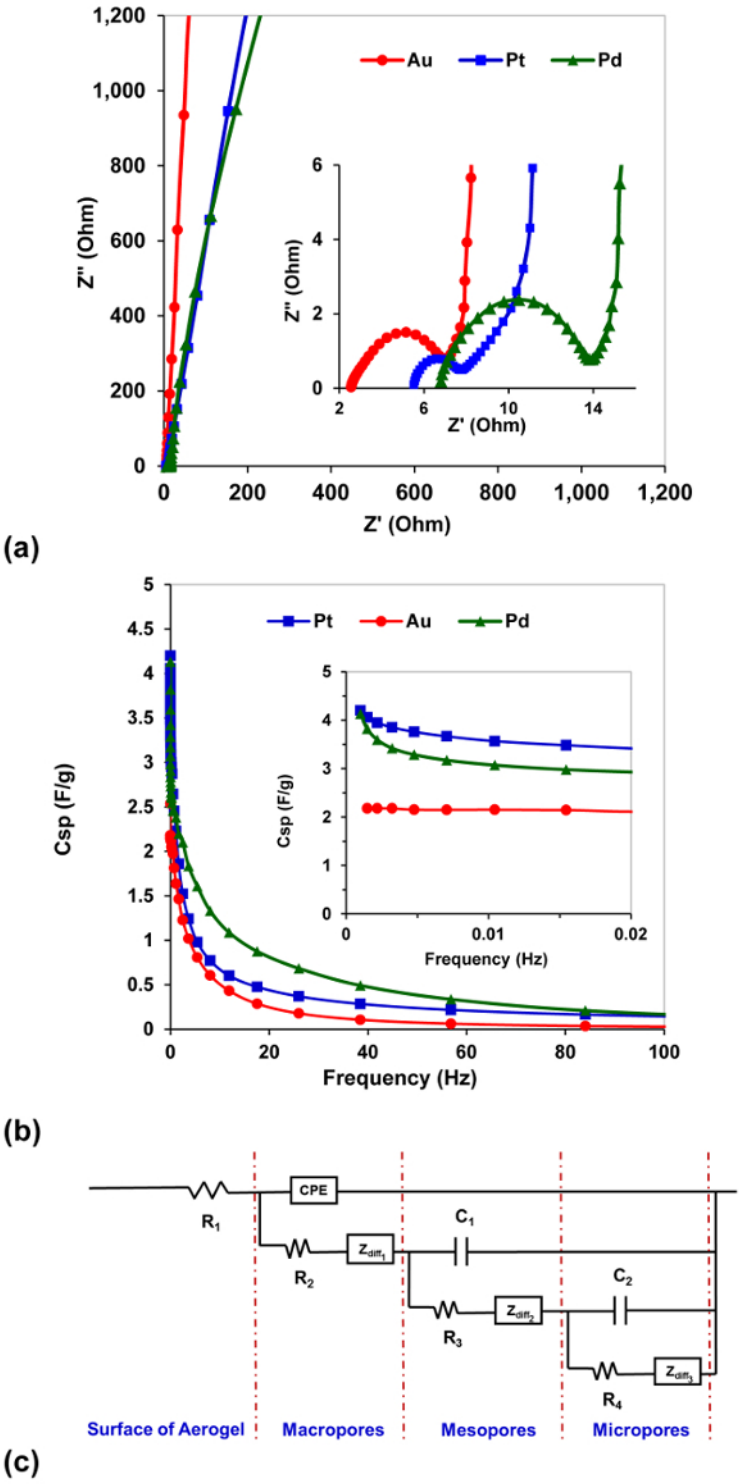

Figure 7. (a) Electrochemical impedance spectra for gold, palladium, and platinum gels performed in 0.5 M KCl vs Ag/AgCl reference electrode. (a) (inset) Low frequency EIS spectra from (a). (b) Specific capacitance (C_{sp}) for gels calculated from low frequency EIS spectra in (a). (b) (inset) Low frequency C_{sp} values. (c) RLC fitted transmission line model (TLM) for EIS spectra. Reproduced from reference 24 with permission. Please click here to view a larger version of this figure.

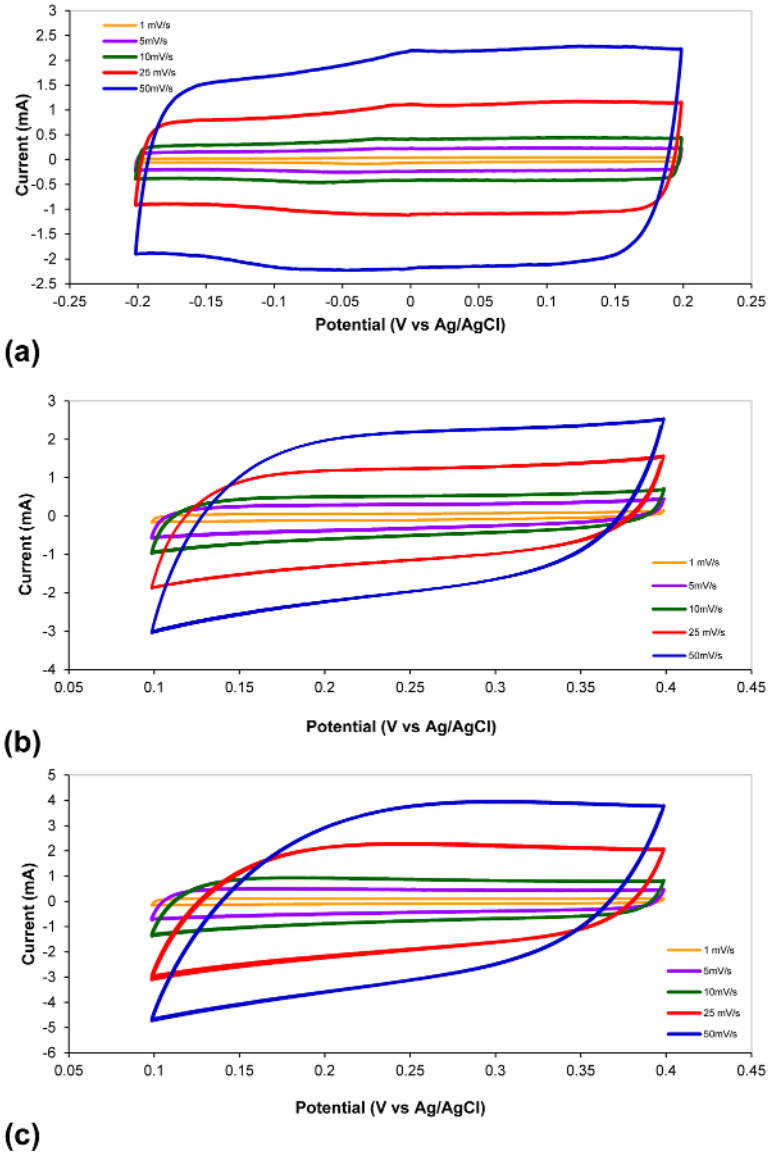

Figure 8. Cyclic voltammetry at scan rates of 50, 25, 10, 5, and 1 mV/s for (a) gold, (b) palladium, and (c) platinum gels. Voltage windows are (a) -0.2 V to 0.2 V, and (b)-(c) 0.1 V to 0.4 V (vs Ag/AgCl). Reproduced from reference 24 with permission. Please click here to view a larger version of this figure.

Discussion

The noble metal aerogel synthesis method presented here results in the rapid formation of porous, high surface area monoliths that are comparable to slower synthesis techniques. The 1:1 (v/v) metal ion solution to reducing agent solution ratio is critical in facilitating the proposed gel formation model. The rapid hydrogen gas evolution as a by-product of the electrochemical reduction of metal ions serves as a secondary reducing agent and facilitates the densification, and fusion of growing nanoparticles during gel formation. Selection of the optimal combinations of metal ion types and reducing agents is also important given that many synthesis combinations shown in **Table 1** do not result in gel formation.

Critical to preserving the gel structure subsequent to chemical reduction is to ensure that gel contact with the solution liquid-air surface is minimized in order to prevent compaction of the gel due to surface tension and capillary forces from water. Extended reduction and rinse times beyond those specified in the protocol may result in further compaction of the metal gels due to continued surface free energy minimization.

The presented synthesis method's primary benefit is the rapid formation of noble metal aerogels with feature sizes commensurate with slower synthesis techniques. The gel feature sizes are achieved without the use of preformed nanoparticles or capping agents during synthesis. Further the experimental correlation of pore and ligament sizes, and surface areas between SEM, XRD, nitrogen gas adsorption, EIS, and CV measurements suggests meaningful and reproducible values.

The protocol may be varied to scale up for the formation of larger aerogels by the use of 15 mL conical tubes with a 3 mL total reaction volume. However, increased reaction volumes are observed to yield increasing variability of final aerogel shape. This increased variability suggests that the aspect ratio of the reaction vessel relative to reaction volume is an important synthesis method consideration. While the primary benefit of the method is rapid gel formation, the lack of shape control reflects the most significant shortcoming for both small and large scale reactions. Future work includes the use of biotemplating and carbon composites as possible approaches to better achieve shape control[35,36]. As a rationally designed scaffold for metal reduction, biotemplated and composite materials may provide further control over ligament length, diameter, and aerogel shape. The direct and rapid synthesis method presented here offers an advancement in decreasing synthesis steps and times to achieve high specific surface areas, and offers a material approach for energy, catalysis, and sensor applications.

Disclosures

The authors have nothing to disclose.

Acknowledgements

The authors are grateful to Stephen Steiner at Aerogel Technologies for his inspiration and technical insights, and to Dr. Deryn Chu at the Army Research Laboratory-Sensors and Electron Devices Directorate, Dr. Christopher Haines at the Armament Research, Development and Engineering Center, U.S. Army RDECOM-ARDEC, and Dr. Stephen Bartolucci at the U.S. Army Benet Laboratories for their assistance. This work was supported by a Faculty Development Research Fund grant from the United States Military Academy, West Point.

References

1. Rolison, D. Catalytic Nanoarchitectures-the Importance of Nothing and the Unimportance of Periodicity. *Science.* **299**, 1698-1701 (2003).
2. Wei, T., Chen, C., Chang, K., Lu, S., Hu, C. Cobalt Oxide Aerogels of Ideal Supercapacitive Properties Prepared with an Epoxide Synthetic Route. *Chemistry of Materials.* **21**, 3228-3233 (2009).
3. Anderson, M., Morris, C., Stroud, R., Merzbacher, C., Rolison, D. Colloidal Gold Aerogels: Preparation, Properties, and Characterization. *Langmuir.* **15**, 674-681 (1999).
4. Gaponik, N., Herrmann, A., Eychmuller, A. Colloidal Nanocrystal-Based Gels and Aerogels: Material Aspects and Application Perspectives. *Journal of Physical Chemistry Letters.* **3**, 8−17 (2012).
5. Olsson, R., *et al.* Making flexible magnetic aerogels and stiff magnetic nanopaper using cellulose nanofibrils as templates. *Nature Nanotechnology.* **5**, 584-588 (2010).
6. Anderson, M., Morris, C., Stroud, R., Merzbacher, C., Rolison, D. Colloidal Gold Aerogels: Preparation, Properties, and Characterization. *Langmuir.* **15**, 674-681 (1999).
7. Gaponik, N., Herrmann, A., Eychmuller, A. Colloidal Nanocrystal-Based Gels and Aerogels: Material Aspects and Application Perspectives. *Journal of Physical Chemistry Letters.* **3**, 8−17 (2012).
8. Hodge, A., Hayes, J., Cao, J., Biener, J., Hamza, A. Characterization and Mechanical Behavior of Nanoporous Gold. *Advanced Engineering Materials.* **8**, 853-857 (2006).
9. Hodge, A., *et al.* Scaling equation for yield strength of nanoporous open-cell foams. *Acta Materialia.* **55**, 1343-1349 (2007).
10. Ambrosi, A., Chua, C., Bonanni, A., Pumera, M. Electrochemistry of Graphene and Related Materials. *Chemical Reviews.* **114**, 7150−7188 (2014).
11. Maillard, F., *et al.* Influence of particle agglomeration on the catalytic activity of carbon-supported Pt nanoparticles in CO monolayer oxidation. *Physical Chemistry Chemical Physics.* **7**, 385-393 (2005).
12. Zhao, P., Li, N., Astruc, D. State of the art in gold nanoparticle synthesis. *Coordination Chemistry Reviews.* **257** 638- 665 (2013).
13. Wen, D., *et al.* Controlling the Growth of Palladium Aerogels with High-Performance toward Bioelectrocatalytic Oxidation of Glucose. *Journal of American Chemical Society.* **136**, 2727−2730 (2014).
14. Jana, N., Gearheart, L., Murphy, C. Seed-Mediated Growth Approach for Shape-Controlled Synthesis of Spheroidal and Rod-like Gold Nanoparticles Using a Surfactant Template. *Advanced Materials.* **13**, 1389-1392 (2001).
15. Ding, Y., Chen, M., Erlebacher, J. Metallic Mesoporous Nanocomposites for Electrocatalysis. *Journal of American Chemical Society.* **126**, 6876-6877 (2004).
16. Liu, W., *et al.* High-Performance Electrocatalysis on Palladium Aerogels. *Angewandte Chemie. International Edition.* **51**, 5743 -5747 (2012).
17. Herrmann, A., *et al.* Multimetallic Aerogels by Template-Free Self-Assembly of Au, Ag, Pt, and Pd Nanoparticles. *Chemistry of Materials.* **26**, 1074−1083 (2014).
18. Ameen, K., Rajasekharan, T., Rajasekharan, M. Grain size dependence of physico-optical properties of nanometallic silver in silica aerogel matrix. *Journal of Non-Crystalline Solids.* **352**, 737-746 (2006).
19. Qin, G., *et al.* A Facile and Template-Free Method to Prepare Mesoporous Gold Sponge and Its Pore Size Control. *Journal of Physical Chemistry C.* **112**, 10352-10358 (2008).
20. Krishna, K., Sandeep, C., Philip, R., Eswaramoorthy, M. Mixing Does the Magic: A Rapid Synthesis of High Surface Area Noble Metal Nanosponges Showing Broadband Nonlinear Optical Response. *ACS Nanotechnology.* **5**, 2681-2688 (2010).
21. Kistler, S. Coherent Expanded Aerogels and Jellies. *Nature.* **127**, 741-741 (1931).
22. Du, A., Zhou, B., Zhang, Z., Shen, J. A Special Material or a New State of Matter: A Review and Reconsideration of the Aerogel. *Materials.* **6**, 941-968 (2013).
23. Tappan, B., Steiner, S., Luther, E. Nanoporous Metal Foams. *Angewandte Chemie. International Edition.* **49**, 4544 - 4565 (2010).
24. Burpo, F., *et al.* Direct solution-based reduction synthesis of Au, Pd, and Pt aerogels. *Journal of Materials Research.* **32**, 4153-4165 (2017).
25. Ostwald, W. Blocking of *Ostwald* ripening allowing long-term stabilization. *PhysicalChemistry.* **37**, 385. (1901).
26. Wang, S., Tseng, W. Aggregate structure and crystallite size of platinum nanoparticles synthesized by ethanol reduction. *Journal of Nanoparticle Research.* **11**, 947-953 (2009).
27. Schneider, C., Rasband, W., Eliceiri, K. NIH Image to ImageJ: 25 years of image analysis. *Nature Methods.* **9,** 671-675 (2012).

28. Thommes, M., *et al.* Physisorption of gases, with special reference to the evaluation of surface area and pore size distribution (IUPAC Technical Report). *Pure and Applied Chemistry.* **87**, 1051-1069 (2015).
29. Barrett, E., Joyner, L., Halenda, P. The Determination of Pore Volume and Area Distributions in Porous Substances. I. Computations from Nitrogen Isotherms. *Journal of the American Chemical Society.* **73,** 373-380 (1951).
30. Brunauer, B., Emmett, P., Teller, P. Adsorption of Gases in Multimolecular Layers. *Journal of the American Chemical Society.* **60,** 309-319 (1938).
31. Herrmann, A., *et al.* Multimetallic Aerogels by Template-Free Self-Assembly of Au, Ag, Pt, and Pd Nanoparticles. *Chemistry of Materials.* **26**, 1074−1083 (2014).
32. Kornyshev, A., Irbakh, M. Double-layer capacitance on a rough metal surface. *Physical Review E.* **53**, 6192-6199 (1996).
33. Bisquert, J. Influence of the boundaries in the impedance of porous film electrodes. *Physical Chemistry Chemical Physics.* **2**, 4185-4192 (2000).
34. Bisquert, J. Theory of the Impedance of Electron Diffusion and Recombination in a Thin Layer. *Journal of Physical Chemistry B.* **106**, 325-333 (2002).
35. Lu, K., Yuan, L., Xin, X., Xu, Y. Hybridization of graphene oxide with commercial graphene for constructing 3D metal-free aerogel with enhanced photocatalysis. *Applied Catalysis B.* 226, 16-22 (2018).
36. Nystron, G., Roder, L., Fernandez-Ronco, M., Mezzenga, R. Amyloid Templated Organic Inorganic Hybrid Aerogels. *Advanced Functional Materials.* 1703609-1703620 (2017).

